SRNL-STI-2014-00514
Rev. 0

DESTRUCTIVE EXAMINATION OF SHIPPING PACKAGE 9975-06100

W. L. Daugherty

Savannah River National Laboratory
Materials Science & Technology

Publication Date: November 2014

Savannah River Nuclear Solutions
Savannah River Site
Aiken, SC 29808

This document was prepared in conjunction with work accomplished under Contract No. DE-AC09-08SR22470 with the U.S. Department of Energy.

DISCLAIMER

DESTRUCTIVE EXAMINATION OF SHIPPING PACKAGE 9975-06100

APPROVALS:

W. L. Daugherty _____ Date _____
Author, Materials Science and Technology

T. E. Skidmore _____ Date _____
Technical Review, Materials Science and Technology

K. A. Dunn _____ Date _____
Pu Surveillance Program Lead, Materials Science and Technology

G. T. Chandler _____ Date _____
Manager, Materials App & Process Tech

E. R. Hackney _____ Date _____
NMM Engineering

REVIEWS:

D. R. Leduc _____ Date _____
Savannah River Packaging Technology

J. W. McEvoy _____ Date _____
9975 Shipping Package Design Authority

Revision Log

Document No. SRNL-STI-2014-00514 **Rev. No.** 0

Document Title Destructive Examination of Shipping Package 9975-06100

Rev. #	Page #	Description of Revision	Date
0	all	Original document	11/7/2014

Nomenclature

ASTM – American Society for Testing and Materials

DSA – Documented Safety Analysis

FT-IR – Fourier Transform Infrared Spectroscopy

ID – Inside Diameter

KAC – K-Area Complex

OD – Outside Diameter

PCV - Primary Containment Vessel

RH – Relative Humidity

SAT – Satisfactory

SCV – Secondary Containment Vessel

SEM – Scanning Electron Microscope

SPA – Surveillance Program Authority

SRNL – Savannah River National Laboratory

SRS – Savannah River Site

UNSAT – Unsatisfactory

WME – Wood Moisture Equivalent

Destructive Examination of Shipping Package 9975-06100

Summary

Destructive and non-destructive examinations have been performed on specified components of shipping package 9975-06100. This package was selected for examination based on several characteristics:

- This was the first destructively examined package in which the fiberboard assembly was fabricated from softwood fiberboard.
- The package contained a relatively high heat load to contribute to internal temperature, which is a key environmental factor for fiberboard degradation.
- The package has been stored in the middle or top of a storage array since its receipt in K-Area, positions that would contribute to increased service temperatures.

No significant changes were observed for attributes that were measured during both field surveillance and destructive examination. Except for the axial gap, all observations and test results met identified criteria, or were collected for information and trending purposes. The axial gap met the 1 inch maximum criterion during field surveillance, but was just over the criterion during SRNL measurements. When re-measured at a later date, it again met the criterion. The bottom of the lower fiberboard assembly and the drum interior had two small stains at matching locations, suggestive of water intrusion. However, the fiberboard assembly did not contain any current evidence of excess moisture. No evidence of a degraded condition was found in this package. Despite exposure to the elevated temperatures of this higher-then-average wattage package, properties of the fiberboard and O-rings are consistent with those of new packages.

Introduction

The Savannah River Site (SRS) stores packages containing plutonium (Pu) materials in the K-Area Complex (KAC). The Pu materials are packaged per the DOE 3013 Standard and stored within Model 9975 shipping packages in KAC.

The KAC facility DSA (Document Safety Analysis) [1] credits the Model 9975 package to perform several safety functions, including criticality prevention, impact resistance, containment, and fire resistance to ensure the plutonium materials remain in a safe configuration during normal and accident conditions. The Model 9975 package is expected to perform its safety function for at least 15 years in the storage environment. The DSA recognizes the degradation potential for the materials of package construction over time in the KAC storage environment and requires an assessment of materials performance to validate the assumptions of the analysis and ultimately predict service life.

As part of the comprehensive Model 9975 package surveillance program [2-3], destructive examination of package 9975-06100 was performed following field surveillance in accordance with Reference [4]. Field surveillance of the Model 9975 package in KAC included nondestructive examination of the drum, fiberboard, lead shield and containment vessels [5]. Results of the field surveillance are provided in Attachment 1.

Package History

Package 9975-06100 was loaded with plutonium oxide material packaged in accordance with DOE-STD-3013 on January 30, 2009 at Hanford. The contents generated approximately 12.2 watts heat load. This package was received in KAC on March 31, 2009. Routine field surveillance was performed on July 24, 2014. SRNL received the package on August 6, 2014 and performed destructive examination activities between August 12 and October 6, 2014.

Package 9975-06100 was fabricated soon after several changes were made to the design requirements. These changes include:

- The lead shield contains a stainless steel sleeve around the outside, which was not included the earlier packages,
- Softwood fiberboard was identified as an acceptable substitute for cane fiberboard in the overpack fiberboard assembly, and
- Viton® GLT-S was identified as an acceptable substitute for Viton® GLT in the containment vessel O-rings.

Visual examination of 9975-06100 confirmed that the shield modification and softwood fiberboard substitution were implemented. It was assumed (and subsequently confirmed through the data collected) that the O-rings were fabricated from Viton® GLT-S.

Discussion

The results of the field surveillance [6] were reviewed. No unsatisfactory conditions were noted. As the package was opened and components removed, each component was marked to identify its orientation within the package. For components that were removed during the field surveillance, their orientation at the time of this examination probably bears no relation to their orientation while stored in KAC. However, the bottom fiberboard subassembly and lead shield would likely have remained in the same orientation they occupied in KAC.

Examination activities are documented through photographs, data sheets, and other documents. This documentation is maintained in a laboratory notebook [7]. The following examination activities were performed:

Fiberboard physical properties:

The weight and dimensions of the top and bottom fiberboard subassemblies were measured. The weight of the top subassembly was 12.080 kg (26.63 lb). During the field surveillance, the measured weight of the top subassembly was 26.7 lb. These two values are in good agreement. Weight and dimension data are recorded in Table 1.

The air shield was cut and peeled back at four locations to permit accurate measurement of the top fiberboard subassembly dimensions. In order to calculate the density of each subassembly, nominal dimensions were assumed for the aluminum bearing plate and air shield. The calculated densities (0.262 g/cc top subassembly, 0.282 g/cc bottom subassembly) meet the limit for the criticality control function, 0.20 g/cc minimum [4]. The volume and density were calculated using the following equations (see the Table 1 sketch for dimension nomenclature).

Top subassembly fiberboard volume,

$V_U = (UD1)^2 (UH1) (\pi/4) + [(UD1) – 2 (UR2)]^2 (UH2) (\pi/4)$
$- (UD2)^2 (UH3) (\pi/4) – 59.96 \text{ inch}^3$

Top subassembly fiberboard weight, W_U = upper subassembly weight – 9.773 lb

Top subassembly fiberboard density, $\rho_U = W_U / V_U$

Bottom subassembly fiberboard volume,

$V_L = (LD1)^2 (LH1) (\pi/4) - [(LD2) + 2 (LR1)]^2 (LH3) (\pi/4)$
$- (LD2)^2 (LH2) (\pi/4) – 59.96 \text{ inch}^3$

Bottom subassembly fiberboard weight, W_L = bottom subassembly weight – 4.827 lb

Bottom subassembly fiberboard density, $\rho_L = W_L / V_L$

Fiberboard dimensions measured during field surveillance are summarized in Attachment 1, and are consistent with drawing requirements and destructive examination measurements. For each of the dimensions measured in both the field surveillance and destructive examination, the measured values are similar. The dimensions were measured twice during destructive examination, 19 and 34 days after the field surveillance. No significant observations were found with the fiberboard physical measurements.

Fiberboard visual appearance:

No significant material or physical damage was observed, and layers were well bonded. The lower subassembly was snug within the drum, but came out smoothly without interference. Following removal of both the top and bottom fiberboard subassemblies from the outer drum, both were inspected visually. Two regions were observed on the bottom of the lower fiberboard assembly, consistent with water stains. Matching stains were observed on the drum bottom interior surface. Some vertical stains were also observed on the drum sides, consistent with water movement, although these did not align with the stains on the bottom. It is hypothesized that a modest amount of water may have run down the side, traveled around the bottom crevice to a point where the fiberboard was compressed into the drum bottom crevice sufficiently to wick up the moisture. The fiberboard and drum stains are shown in Figures 1-3.

Fiberboard moisture content:

The moisture content of the fiberboard will affect its properties, including density, mechanical strength and thermal properties. Measuring the moisture content of the top and bottom subassemblies, and the relative humidity inside the package, provides reference data to potentially correlate laboratory test results with behavior in KAC. The fiberboard moisture content was measured twice during destructive examination activities – upon receipt of the package, and again approximately 2 weeks later. Measurements were also taken during field surveillance to the extent the fiberboard was accessible.

A GE Protimeter Surveymaster moisture probe was used to measure the moisture content of the top and bottom fiberboard subassemblies. This probe identifies the wood moisture equivalent (WME), or the weight % of moisture that would produce the same electrical conductivity in wood. Moisture content data are presented in Figure 4.

Moisture measurements were compared to those taken during previous destructive examinations [8 – 14]. The readings on 9975-06100 are lower on average than seen on previous DE packages, although 9975-03431 had similar low readings. During field surveillance, the measured moisture content of accessible regions of the fiberboard ranged from 6 to 11 %WME. During subsequent examination, with both upper and lower fiberboard assemblies removed, moisture content ranged from 6.2 to 14.5 %WME. The highest moisture content was measured under the air shield, which was not accessible during field surveillance.

A moisture gradient of 4.3 %WME was observed across the upper fiberboard assembly side wall during field surveillance. During the subsequent inspections, this gradient decreased to 2.9 %WME. The moisture gradient across the lower assembly side wall was not recorded during field surveillance, but was 3.8 %WME 19 days later, and 3.5 %WME 34 days later. This is consistent with other packages examined – the larger moisture gradient tends to develop in the lower assembly, and the gradient in both assemblies decreases gradually after the internal heat load is removed.

Consistent with recent efforts to correlate moisture content of fiberboard with humidity in the surrounding air, data were taken to correlate these two parameters. The fiberboard was placed back in the drum with a narrow channel cut down the side. A humidity probe was placed in this channel such that it could be raised and lowered with the drum closed. The edge of the drum lid was taped to seal around the gap created by the humidity probe cable. After humidity levels in the drum reached equilibrium, humidity readings were taken at several elevations along the fiberboard, and the fiberboard was then removed to measure the moisture content at those same locations. This process was repeated to demonstrate consistency in the results. These data are summarized in Figure 5, and compared to similar data from three previous DE packages and laboratory samples. All the prior data were generated with cane fiberboard, and show a similar trend, with the data for the 9975 packages offset slightly from that for laboratory samples. The current data from 9975-06100 are shifted slightly from the other 9975 DE packages, but are in good agreement with the cane fiberboard laboratory samples. Additional data will be needed from softwood fiberboard laboratory samples to identify whether there is a general offset in behavior between cane and softwood fiberboard.

Fiberboard thermal and mechanical properties:

Samples of fiberboard were removed from the bottom fiberboard subassembly to measure compressive strength, specific heat capacity and thermal conductivity. The source location(s) of these samples is illustrated in Figures 6 and 7. The thermal conductivity sample from the bottom center of the subassembly is oriented for heat flow in the axial direction (perpendicular to the glue joints). The thermal conductivity sample from the side is oriented for heat flow in the radial direction (parallel to the glue joints). Testing on each sample was performed at a nominal (mean) temperature of approximately 25ºC (77ºF), with no environmental conditioning. Physical data on the fiberboard samples are recorded in Table 2.

The compression test data are shown in Figures 8 and 9, along with baseline data for a different softwood fiberboard assembly. For both the perpendicular and parallel orientations, the

compression strength of the 9975-06100 samples is similar to the baseline samples. A series of photographs showing typical compression behavior under parallel loading is shown in Figure 10. The area under the stress-strain curve up to 40% strain is used as a relative indication of the energy absorption capacity of the fiberboard. This metric is shown in Figure 11 for each destructively examined package as a function of fiberboard moisture content. In general, the energy absorption capacity decreases as the moisture content increases. The results from 9975-06100 are circled in Figure 11. The Figure 11 data collectively show a trend consistent with undegraded softwood fiberboard and with other DE packages.

A total of four samples were prepared from the side and base of the lower subassembly for measuring the specific heat capacity of the fiberboard. The specific heat capacity was calculated in accordance with ASTM C351 at a mean temperature of ~25ºC (77ºF). This ASTM Standard specifies test temperatures that would produce a mean test temperature of 60ºC, but allows alternate test temperatures to be substituted as needed. Data were collected for a sample target temperature of 45ºC, and a water temperature of ~5ºC. The sample moisture content was 6.0 – 9.2 % WME (wood moisture equivalent). Each sample was tested three times, and all results were averaged. The average specific heat capacity value was 1311 J/kg-K. Multiplying this value by the density of the lower subassembly (282 kg/m^3) gives a heat capacity of 370,000 J/m^3-K (5.5 Btu/ft^3-F). This meets the required minimum value of 3 Btu/ft^3-F. The specific heat capacity value is slightly lower than typical compared to baseline laboratory data, but consistent with previous DE packages.

The thermal conductivity of the fiberboard was measured with a Lasercomp Inc. Fox 300 thermal conductivity instrument at a mean temperature of 25ºC (77ºF). For the sample with axial heat flow (perpendicular to the fiberboard layers), the measured thermal conductivity is 0.0574 W/m-K (0.0332 Btu/hr-ft-ºF). For the sample with radial heat flow (parallel to the fiberboard layers), the measured thermal conductivity is 0.1030 W/m-K (0.0595 Btu/hr-ft-ºF). Both thermal conductivity values fall within the identified range [4], and are consistent with typical baseline laboratory data [15, 16].

Lead shield visual examination:

The entire surface of the lead shield was visually examined. It was found to be free from significant deformation and physical damage. The exterior stainless steel sleeve protects the lead surface, and precludes direct visual examination of the lead. Lead is visible only on the top edge, and in this area there was no significant corrosion or degradation (Figure 12).

Lead Shield Dimensions:

Several lead shield dimensions were measured (Table 3) and all are consistent with drawing requirements.

The radial thickness was measured near the top of the shield, and was calculated from diametral data taken near the bottom of the shield. The calculated thickness from near the bottom (0.554 inch) is similar to the measured thickness near the top (0.540 inch). This comparison is made to

indicate whether the lead may have undergone creep during service; however, the outer stainless steel sleeve provided on this shield is expected to minimize the likelihood of creep.

O-ring examination and testing:

Prior surveillance testing of the four O-rings from this package included visual examination, dimensional and hardness measurements. Dimensional measurements were repeated on each O-ring as part of the destructive examination. Three of these O-rings (SCV outer, PCV outer and PCV inner) received additional testing. All three were submitted for FT-IR spectroscopy to confirm material composition, and the two outer O-rings received optical and SEM microscopic examination of the cross section. The dimensions and weight of the SCV outer and PCV outer O-rings were recorded to calculate their density. The PCV inner O-ring was tensile tested, including a hold point at 50% strain to visually examine the O-ring.

Weight and dimension data for the two outer O-rings are presented in Table 4. The average minor diameter for each O-ring is within the specified tolerances for new O-rings, but the major inside diameter for each O-ring (calculated from the length measured after the O-ring was cut) is greater than specified for new O-rings. This is consistent with a permanent stretch due to the lid diameter. Leak testing during the field surveillance successfully demonstrated leak-tightness to a level of approximately 1×10^{-3} std cc air/sec.

Compression set was calculated for each O-ring based on each of the dimensional measurements it received. Compression set is calculated as follows, assuming an initial minor diameter of 0.139 inch and an average groove depth in the lid of 0.0995 inch.

$$\text{Compression set (\%)} = (0.139 - \text{radial thickness}) / (0.139 - 0.0995)*100$$

Since the field surveillance did not include measurement of the O-ring thickness after removal from the plug, the compression set is calculated from measurements using the O-ring diameter as-installed, the subsequently measured plug diameter, and the degree of thinning expected from being stretched by the plug (based on the Parker O-ring Handbook).

Compression set values are shown in Figure 13 as a function of time since removal of the O-rings, for the current package as well as for 9975-02168 and 9975-03431 for comparison. The compression set decreases with time, as the polymer continues to relax. Typically, the compression set has reached an equilibrium value after about 30 days or so. Compression set behavior is similar for each O-ring in these three packages. In the few cases where the compression set is negative, it is likely that the initial O-ring thickness was greater than the nominal 0.139 inch that was assumed.

FT-IR spectroscopy generically identified the composition of each O-ring as consistent with a Viton® type fluoroelastomer (Figure 14). Each O-ring produced a similar FTIR spectrum in the as-received condition (i.e. with some grease residue). Figure 14 (b) compares the spectrum for the PCV inner O-ring before and after wiping off the grease, and shows some of the lower wavelength peaks reduced or eliminated. After wiping, the spectrum is very similar to that of a

new (unused and clean) Viton® GLT-S O-ring shown in Figure 14 (c), and is consistent with baseline data [17].

As with previous destructive examinations, visual (Figure 15) and SEM (Figure 16) examination of the cross sections identified a distribution of very small particles throughout each O-ring. Aside from carbon and fluorine (the primary constituents of Viton® fluoroelastomer) the SEM identified small amounts of magnesium, aluminum, silicon, sulfur, calcium, and oxygen. Though the actual compound is proprietary, Viton®-type fluoroelastomer compounds typically contain MgO, CaO, $Ca(OH)_2$, ZnO or lead compounds as acid acceptors and heat stabilizers [18]. Aluminum is present in hydrotalcite, which is used in both GLT and GLT-S compounds as a filler reinforcing agent. Silicon may be present as a trace contaminant.

The PCV inner O-ring was tensile tested in accordance with ASTM D1414, using a cut (single strand) sample. The test was interrupted at 50% strain (Figure 17) to visually examine the O-ring for signs of cracking or other degradation. None were observed. The initial stress-strain curve for the PCV inner O-ring is shown in Figure 18. In this first test, the O-rings failed after reaching 600% strain, an unusually high value for any Viton® O-ring (GLT, GLT-S, etc), even compounds without reinforcing fillers. A re-test reached 650% elongation without breaking. Comparison tests performed on the PCV outer O-ring and a new O-ring that was re-installed on the PCV also produced higher elongation than expected (450, 530%). Each of these O-rings was tested using a yarn grip which would allow some stretch beyond the gage section. It is theorized that these GLT-S O-rings experienced significantly more stretch beyond the gage section than previous GLT O-rings. To more accurately measure the elongation, tests were performed with an alternate grip arrangement which does not allow such stretch. These alternate flat grips pose a greater risk of breaking within the grips (which would invalidate the test), but they provide a better measure of the elongation. With this arrangement, the PCV inner O-ring had an elongation of 385%, while the new O-ring had an elongation of 359%. Both of these values are similar to baseline data [17]. These comparison tests are also shown in Figure 18. For each of the O-rings tested, the tensile strength ranged from 2.2 to 2.9 ksi, which is comparable to baseline GLT-S data, but higher than prior GLT data.

9975-06100 is the first package from KAC to undergo destructive examination which was assembled with Viton® GLT-S O-rings. The O-rings from 9975-06100 differ from those examined in the past in two regards. First, the hardness is slightly higher (82.6 – 85 Durometer M, compared to ~76 – 80 typical for previous packages and baseline GLT-S O-rings). A similar elevated hardness (82.3) was measured on the new O-ring installed on the PCV that was used for comparative tensile data. Second, some differences were noted in the trace elements identified by SEM, primarily magnesium instead of zinc. It is noted that neither element is formally exclusive of the GLT-S composition. These differences are judged to be not significant with regards to O-ring integrity and service life for a storage application.

General:

A general visual examination was performed on all metallic components. No significant damage or degradation was observed. Several components were observed to have fabrication markings. Various markings were stamped or engraved on the containment vessels and lids. These

markings appear to be identification numbers used during manufacture, prior to association of the parts with a final package number, and are consistent with those seen in other packages. The bottom head of the SCV is darkened on both the interior and exterior surfaces. The interior surface is even darker opposite the support ring attachment welds (Figure 19).

The distance from the drum flange to the top of the air shield was measured, and ranged from 0.985 to 1.027 inch. The average value was 1.0005 inch. During the second examination at SRNL, the average air gap was found to have decreased to 0.984 inch, which meets the acceptance criterion of 1 inch maximum. The drum drawing [19] identifies a reference value for this dimension as 0.8 inch, and notes that it may vary over time due to variations in fiberboard properties. Pre-operational verification requirements, consistent with fire and drop test qualifications for the 9975 package, specify this dimension be no greater than 1 inch. During field surveillance, the average value of this dimension was noted to be less than 1 inch.

The data from the examination activities described above are compared with field surveillance data in Attachment 1. Except for the initial SRNL measurement of the axial gap, all specified criteria were met during this examination. All observations and examination results are consistent with expectations. All findings will be reviewed by NMM for potential impact on the continued storage of other packages in KAC.

Measurement Uncertainties:

Numerous measurements were made with a variety of instruments during the destructive examination of package 9975-03431. Some of the measurements were specifically compared to inspection criteria, while others were taken for information / trending purposes. All measurements which are compared to inspection criteria were made with calibrated instruments, or were verified against calibrated instruments. The uncertainties associated with measurements and calculated results required to meet inspection criteria are discussed below.

Weight – The weight of each fiberboard subassembly was measured to a precision of 2 grams. The balance used was M&TE, and the calibration data show an accuracy within 5 grams over the range of interest. A conservative net uncertainty of 7 grams will be used.

Calipers – Three different calipers were used to measure component dimensions. All three calipers are M&TE, and calibration data show an accuracy within 0.001 inch. In addition, operator bias can affect measurement accuracy through the contact load applied when making a measurement. A degree of give exhibited by the fiberboard will lead to different results as the contact load changes. The larger calipers are judged to be more susceptible to this bias. Metallic components are significantly more rigid than the fiberboard, but operator bias may also exist for those components. While not characterized explicitly, it is judged that the total uncertainty (instrument uncertainty plus operator bias) for fiberboard measurements is no greater than +/- 0.003 inch for the 6 inch calipers, +/- 0.005 inch for the 24 inch calipers, and +/- 0.007 inch for the 40 inch calipers. It is further judged that total uncertainty when measuring metallic components is no greater than +/- 0.003 inch for 6 and 24 inch calipers, and +/- 0.005 inch for the 40 inch calipers.

Manual calipers – Dimension ID2 on the lead shield was captured with manual swing calipers, which was then locked in that position and measured with 24-inch calipers. It is judged that the accuracy of capturing this dimension with the manual calipers is within +/- 0.002 inch, and the measurement of that dimension is then within +/- 0.002 inch, for a (conservatively) combined accuracy of +/- 0.004 inch.

Thermal conductivity instrument – The specifications for the Fox300 thermal conductivity instrument include a stated accuracy of ~1%. Measurement of the thermal conductivity of a calibration standard was accurate to within 1.1%. Prior test reports of fiberboard samples from an independent laboratory, using the same model instrument, identified an overall 3% uncertainty. An uncertainty of 3% will be conservatively assumed for the current measurements.

Heat capacity – The specific heat capacity is derived from temperature and weight measurements, using calibrated instruments. The thermocouple and balance precisions are high. The greatest contribution to error in the specific heat capacity is considered to be consistency of operator technique. The total uncertainty is reflected in the range of results for multiple trials. The heat capacity was measured three times on each of four samples. The variation for each sample ranged from 2.4 to 21%. The combined uncertainty on the average of 4 samples is 8%.

Where measurement results are used in subsequent calculations, the uncertainty values identified above are assumed to be random. A standard error propagation formula for random errors is used to calculate the final result uncertainty. In some cases, the calculated uncertainty may be less than the potential error from rounding off the result, and the higher variation associated with round-off is reported as the uncertainty. These calculations are documented in the Laboratory Notebook [7]. Calculation results and their uncertainties are summarized as follows:

- Top fiberboard subassembly volume = 28871 +/- 26 cm^3
- Top fiberboard subassembly density = 0.265 +/- 0.001 g/ cm^3
- Bottom fiberboard subassembly volume = 85651 +/- 72 cm^3
- Bottom fiberboard subassembly density = 0.283 +/- 0.001 g/ cm^3
- Shield radial thickness at bottom = 0.554 +/- 0.003 inch
- Thermal conductivity (radial) = 0.0595 +/- 0.002 Btu/hr-ft-ºF
- Thermal conductivity (axial) = 0.0332 +/- 0.001 Btu/hr-ft-ºF
- Heat capacity = 5.5 +/- 0.4 Btu/ft^3-ºF

References

[1] WSRC-SA-2002-00005, Rev. 1CN-7, "K-Area Material Storage Facility Documented Safety Analysis", June 2008.

[2] SFS-ENG-99-0085, "Summary and Guide to 9975 Container Qualification Program"

[3] WSRC-TR-2001-0286, Rev. 4, "The Savannah River Site Surveillance Program for the Storage of 9975/3013 Plutonium Packages in KAC", July 2008

[4] WSRC-TR-2005-00135 Rev. 1, "Task Technical and Quality Assurance Plan for Destructive Examination of a 9975 Package from Field Surveillance Activities", W. L. Daugherty, March 2011

[5] WSRC-TR-2004-00197, "Inspection Activities and Acceptance Criteria for Field Surveillance of Model 9975 Package O-Rings and Celotex® Materials", W. L. Daugherty, April 2004

[6] SOP-CSS-207-K, Rev. 9, Attachment 2 "9975 Surveillance Data Sheet" for 9975-06100

[7] SRNL-NB-2012-00048, Laboratory Notebook "9975 Shipping Package Celotex Testing Book IV

[8] WSRC-TR-2005-00273, Rev. 1, "Destructive Examination of Shipping Package 9975-02234", W. L. Daugherty, September 2005

[9] WSRC-TR-2006-00162, "Destructive Examination of Shipping Package 9975-00826", W. L. Daugherty, May 2006

[10] WSRC-STI-2007-00558, "Destructive Examination of Shipping Package 9975-00600", W. L. Daugherty, October 2007

[11] SRNS-STI-2008-00019, "Destructive Examination of Shipping Package 9975-05128", W. L. Daugherty, August 2008

[12] SRNL-STI-2009-00763, "Destructive Examination of Shipping Package 9975-02028", W. L. Daugherty and T. M. Stefek, December 2009

[13] SRNL-STI-2010-00654, "Destructive Examination of Shipping Package 9975-02168", W. L. Daugherty, November 2010

[14] SRNL-STI-2012-00257, "Destructive Examination of Shipping Package 9975-03431", W. L. Daugherty, May 2012

[15] SRNL-MST-2008-00043, "Properties of Un-Aged Knight-Celotex Softwood Fiberboard for Thermal Modeling", W. L. Daugherty, February 27, 2008

[16] SRNL-TR-2009-00475, "First Status Report: Testing of Aged Softwood Fiberboard Material for the 9975 Shipping Package", W. L. Daugherty, January 2010

[17] WSRC-TR-2008-00163, "Baseline Characterization of Viton® GLT-S O-Rings for Model 9975 Shipping Packages in KAMS", T. E. Skidmore and E. N. Hoffman, May 2008

[18] Rubber Technology Handbook, W. Hofmann, Hanser Publishers, New York, 1989, page 122

[19] Drawing R-R2-F-0025, Rev. 5, "9975 Drum with Flange Closure Subassembly & Details"

Table 1. Fiberboard physical measurements and calculated density

Top Subassembly						
Weight	12.082 kg					R-R2-F-0019 Rev 5
	0/180 deg.		90/270 deg.		Avg.	Nominal value (inch)
UD1 (in)	17.677		17.684		17.680	17.7
UD2 (in)	8.544		8.532		8.538	8.55
	0 deg.	90 deg.	180 deg.	270 deg.	Avg.	
UR1 (in)	3.067	3.068	3.063	3.069	3.067	3.075
UR2 (in)	1.493	1.500	1.478	1.462	1.483	1.5
UH1 (in)	7.107	7.140	7.134	7.149	7.132	7.1
UH2 (in)	2.132	2.120	2.121	2.113	2.122	2.1
UH3 (in)	5.061	5.063	5.072	5.058	5.064	5.0

Top subassembly calculated density = 0.265 g/cc

Bottom Subassembly						
Weight	26.390 kg					R-R2-F-0019 Rev 5
	0/180 deg.		90/270 deg.		Avg.	Nominal value (inch)
LD1 (in)	18.070		18.072		18.071	18.1
LD2 (in)	8.453		8.443		8.448	8.45
	0 deg.	90 deg.	180 deg.	270 deg.	Avg.	
LR1 (in)	3.300	3.283	3.255	3.249	3.272	3.275
LR2 (in)	1.529	1.522	1.526	1.530	1.527	1.55
LH1 (in)	26.526	26.582	26.544	26.514	26.542	26.7
LH2 (in)	20.531	20.561	20.553	20.517	20.540	20.4
LH3 (in)	2.101	2.110	2.084	2.078	2.093	2.0

Bottom subassembly calculated density = 0.283 g/cc

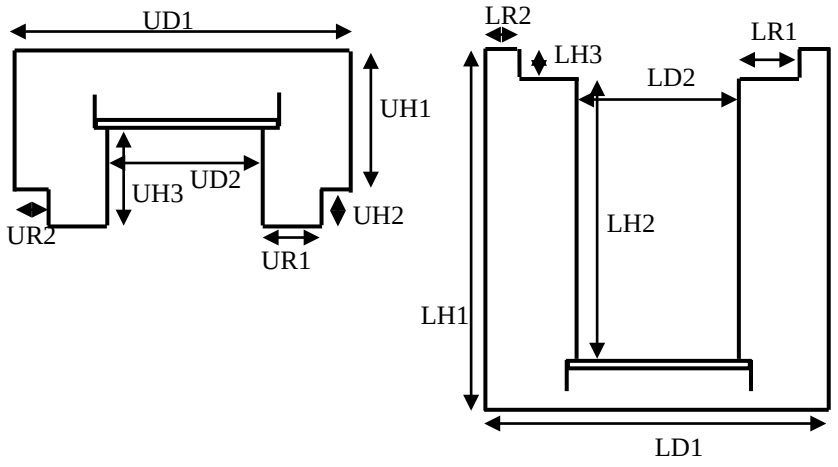

Table 2. Physical data for fiberboard test specimens

Test Sample	Moisture Content (%WME)	Weight (g)	Length (inch)	Width (inch)	Height (inch)	Density (g/cc)
Compression Test Samples						
Side 1 (parallel)	7.4	38.074	2.026	2.019	2.032	0.280
Side 2 (parallel)	7.9	37.161	2.027	2.019	2.031	0.273
Side 3 (perpendicular)	7.4	37.110	2.031	2.022	2.027	0.272
Side 4 (perpendicular)	8.0	38.036	2.029	2.017	2.033	0.279
Base 1 (parallel)	9.0	37.139	2.003	2.001	2.013	0.281
Base 2 (parallel)	9.8	35.854	2.004	1.965	2.004	0.277
Base 3 (perpendicular)	9.6	36.227	2.010	2.006	2.007	0.273
Base 4 (perpendicular)	9.0	36.383	2.012	2.013	2.010	0.273
Thermal Conductivity Samples						
Side (radial)	7.0	267	7.036	6.996	1.211	0.273
Base (axial)	10.2	312	7.035	7.024	1.371	0.281

Table 3. Lead shield dimensions

Dimension	0/180 deg. (inch)		90/270 deg. (inch)		Avg. (inch)	Requirement (inch)
OD (in)	8.334		8.343		8.338	8.252 – 8.35
ID1 (in)	7.283		7.256		7.270	7.25 – 7.26 for non-jacketed shield 7.22 – 7.28 for jacketed shield
ID2 (in)	7.243		7.219		7.231 *	7.24 – 7.26
	0 deg.	90 deg.	180 deg.	270 deg.		
R (in)	0.538	0.552	0.530	0.541	0.540	0.506 min
H (in)	24.676	24.697	24.686	24.682	24.685	24.556 – 24.7

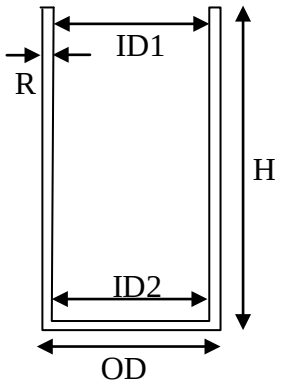

(OD – ID2) / 2 = 0.554 inch

* ID2 re-measured at 4 locations, average value = 7.244 inch

Table 4. O-ring physical data

~60 Days after	PCV Outer O-Ring Thickness		SCV Outer O-Ring Thickness	
Field Surveillance	Radial (inch)	Axial (inch)	Radial (inch)	Axial (inch)
Minor Dia. 0 deg	0.1400	0.1370	0.1345	0.1390
Minor Dia. 45 deg	0.1410	0.1355	0.1390	0.1350
Minor Dia. 90 deg	0.1425	0.1390	0.1405	0.1375
Minor Dia. 135 deg	0.1435	0.1350	0.1415	0.1355
Minor Dia. 180 deg	0.1430	0.1365	0.1405	0.1360
Minor Dia. 225 deg	0.1405	0.1345	0.1400	0.1395
Minor Dia. 270 deg	0.1380	0.1370	0.1415	0.1350
Minor Dia. 315 deg	0.1415	0.1335	0.1345	0.1380
Avg. Minor Dia.	**0.1386**		**0.1380**	
Minor Dia. (new)	0.138 +/- 0.006 inch		0.138 +/- 0.006 inch	
Length (after cut)	14 2/32 inch		17 7/32 inch	
Calculated Major Dia.	4.476 inch avg		5.481 inch avg.	
Major Inside Dia. (new)	4.234 +/- 0.030 inch		5.234 +/- 0.035 inch	
Weight	6.1958 g		7.6790 g	
Calculated Volume	0.212 $inch^3$ (3.477 cm^3)		0.225 $inch^3$ (4.220 cm^3)	
Calculated Density	**1.782 g/cm^3**		**1.819 g/cm^3**	

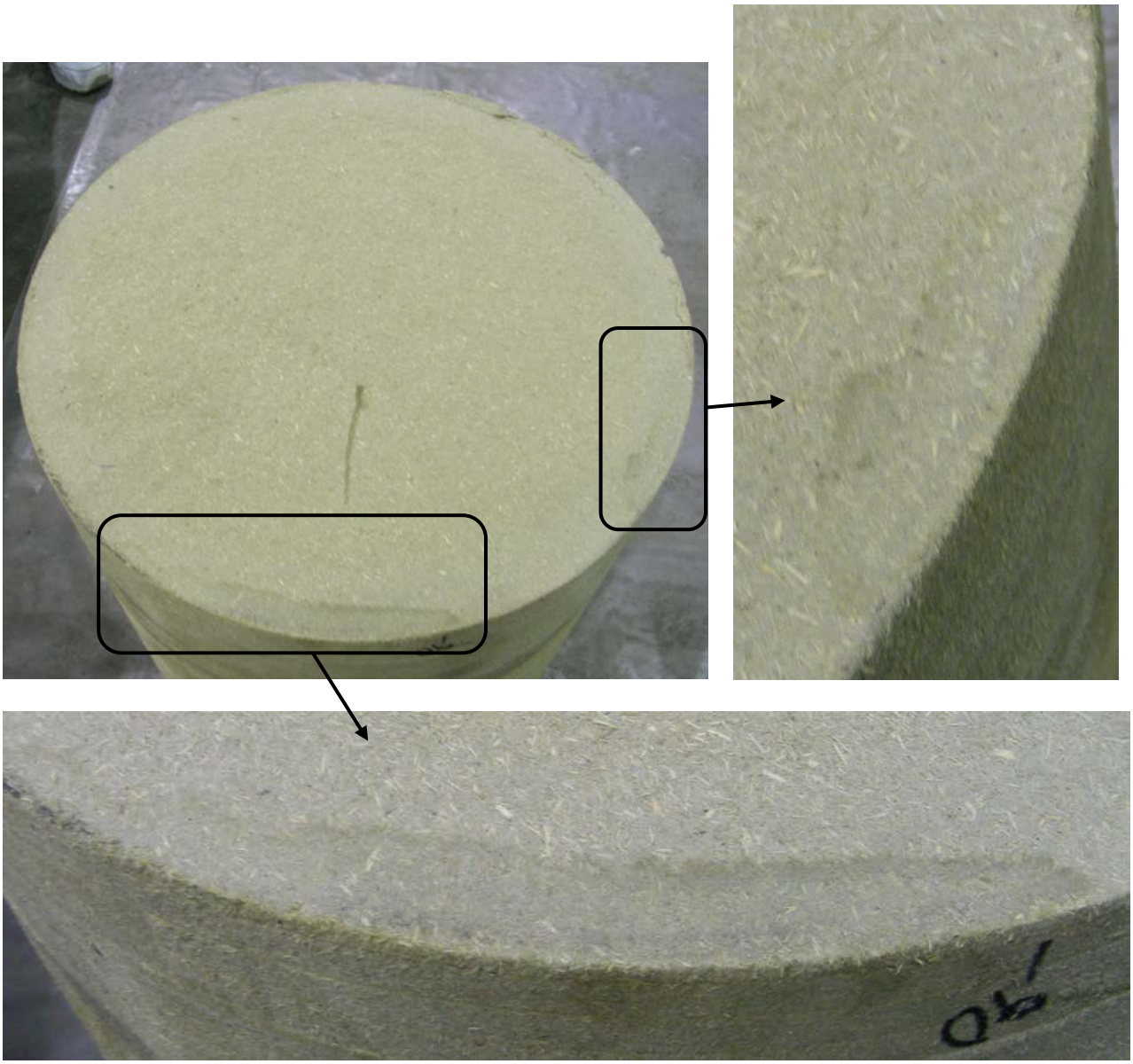

Figure 1. Water stains on lower fiberboard assembly

Figure 2. Water stains on drum bottom corresponding to fiberboard stains

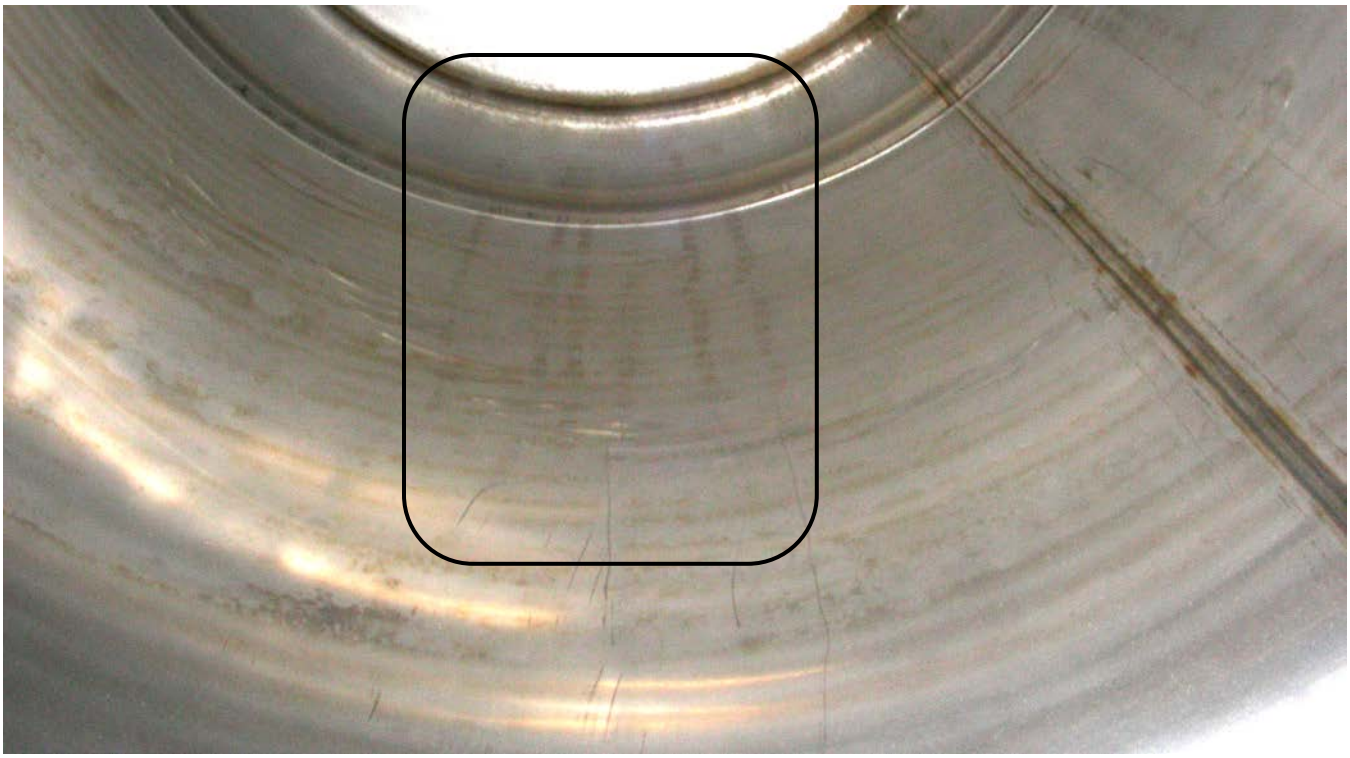

Figure 3. Vertical water stains on drum side

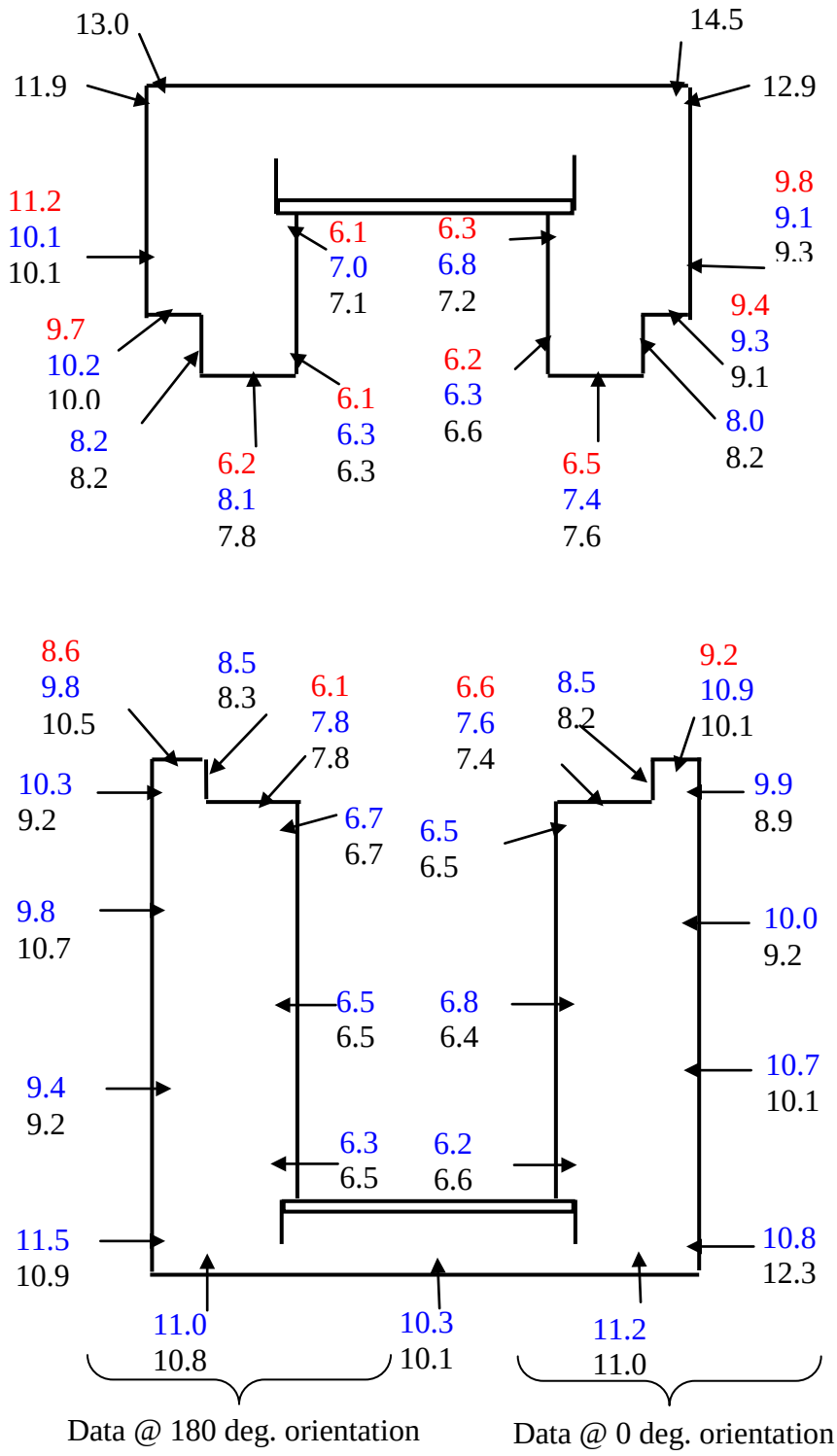

Figure 4. Fiberboard moisture content data. The values in red were measured during field surveillance. The values in blue were measured 19 days later, while the values in black were measured 34 days after field surveillance. All values are % wood moisture equivalent.

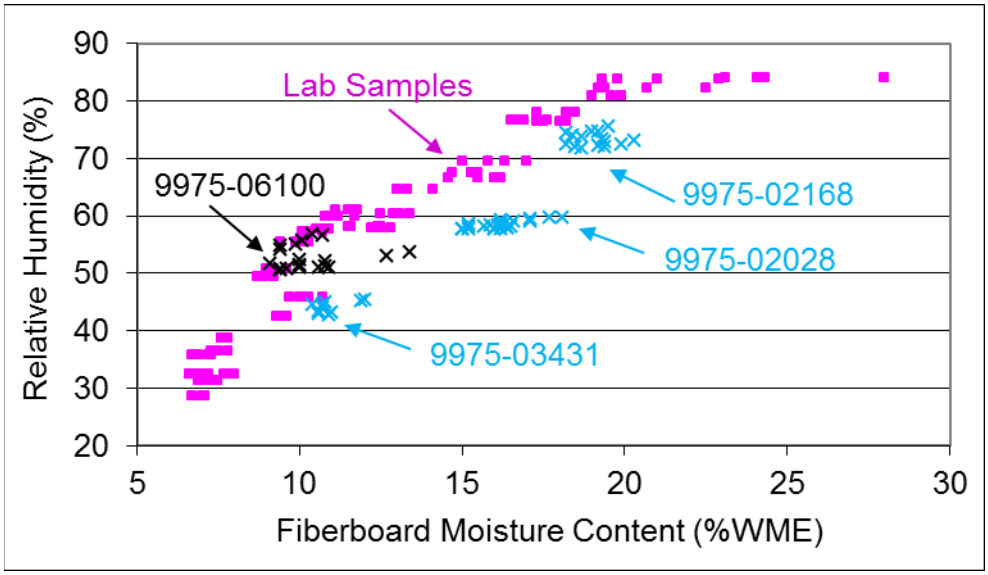

Figure 5. Correlation between fiberboard moisture content and relative humidity of the adjacent air. Data from 9975-06100 are shown with comparable data from prior DE packages and laboratory samples. Measurements were taken along the fiberboard OD surface.

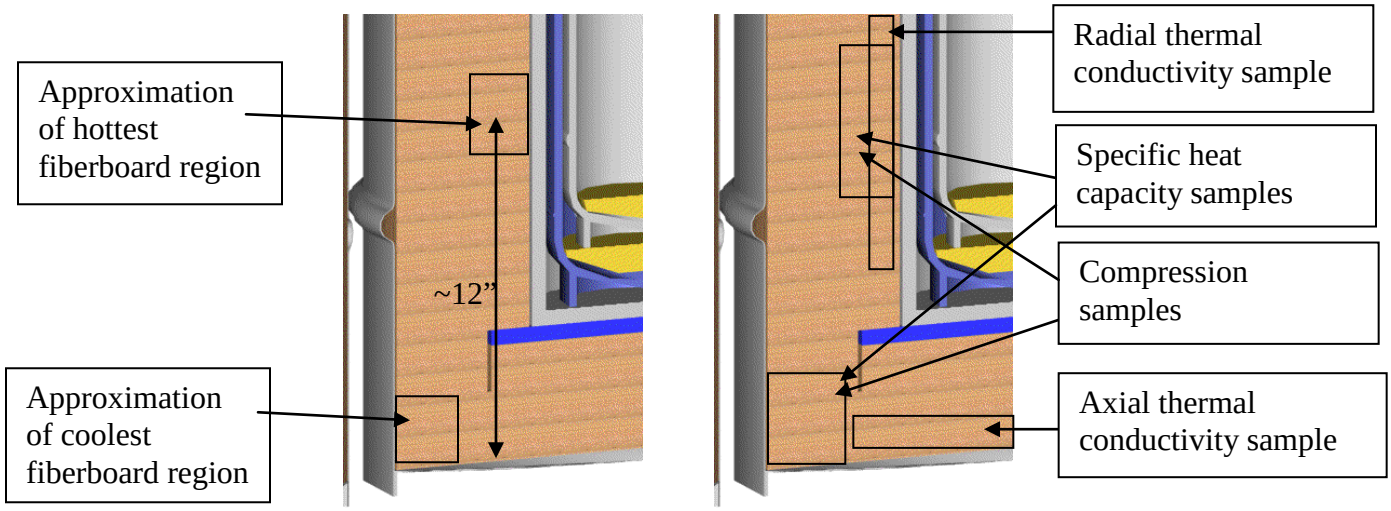

Figure 6. Illustration of fiberboard regions of the bottom subassembly to be tested. Multiple samples (where used) were removed from the illustrated locations at different circumferential positions. Not to scale.

Figure 7. Lower fiberboard assembly marked for removal of test samples

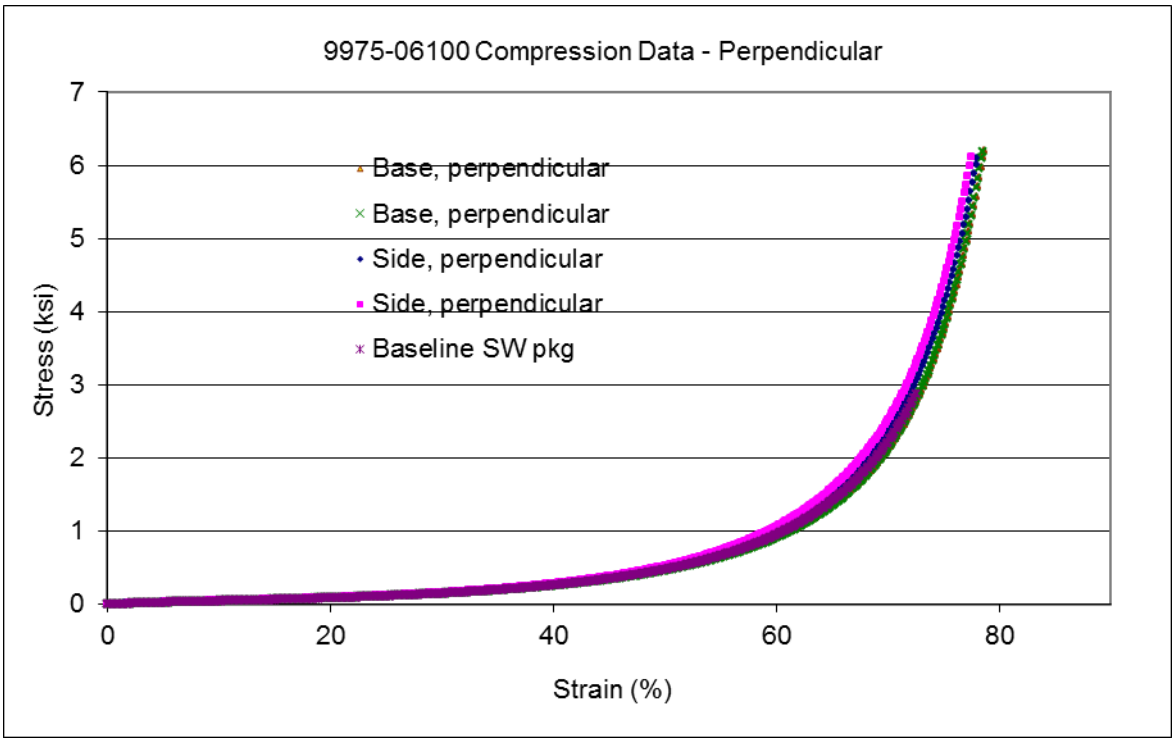

Figure 8. Fiberboard compression test data, compared with typical baseline data from an unaged softwood assembly, in the perpendicular orientation (i.e. load applied perpendicular to the fiberboard layers).

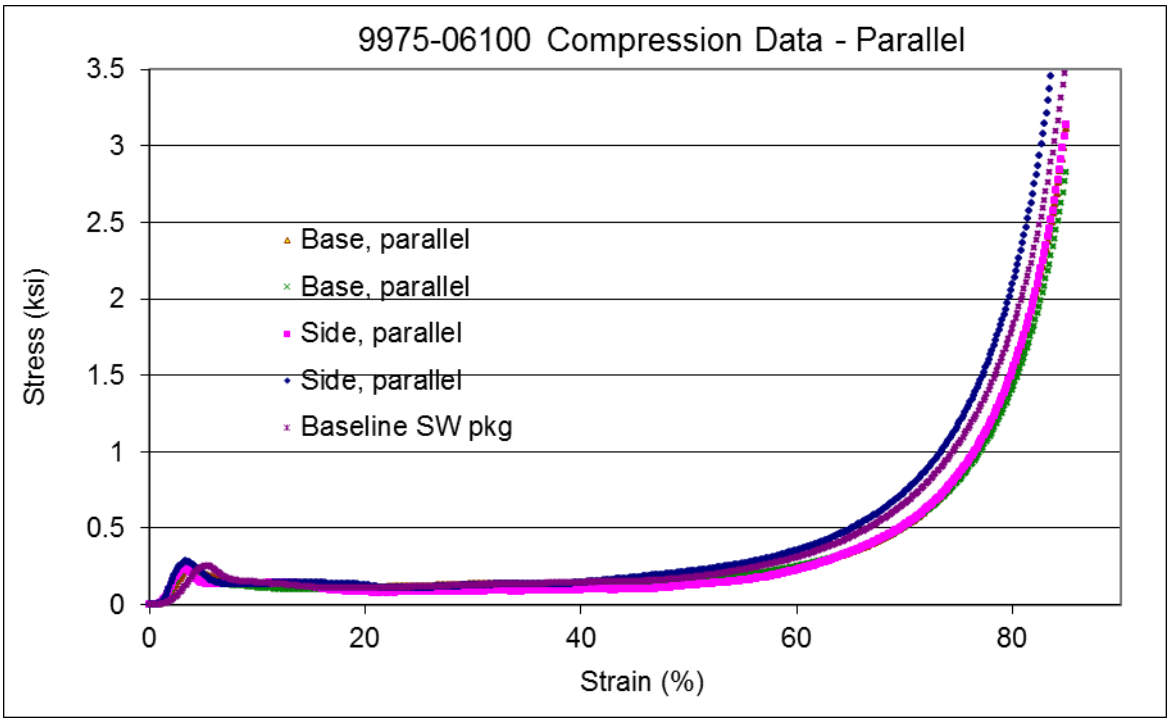

(a)

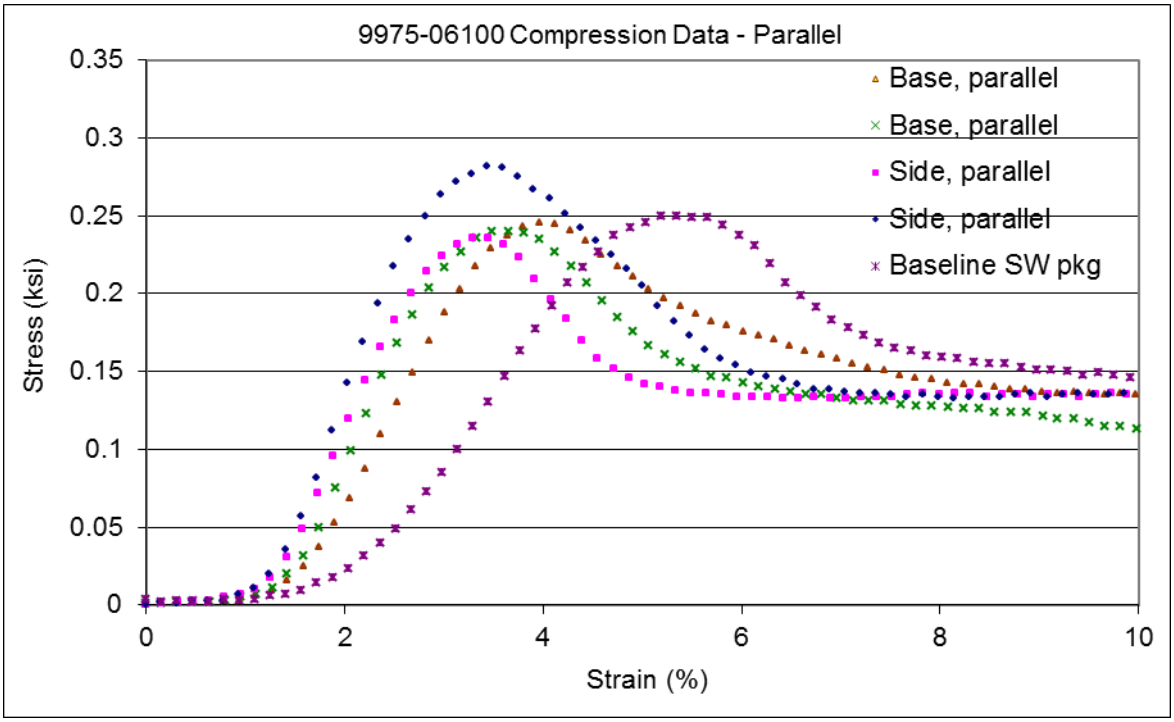

(b)

Figure 9. Fiberboard compression test data, compared with typical baseline data from an unaged softwood assembly, in the parallel orientation (i.e. load applied parallel to the fiberboard layers). The full curves are shown in (a), while the initial buckling region is expanded in (b).

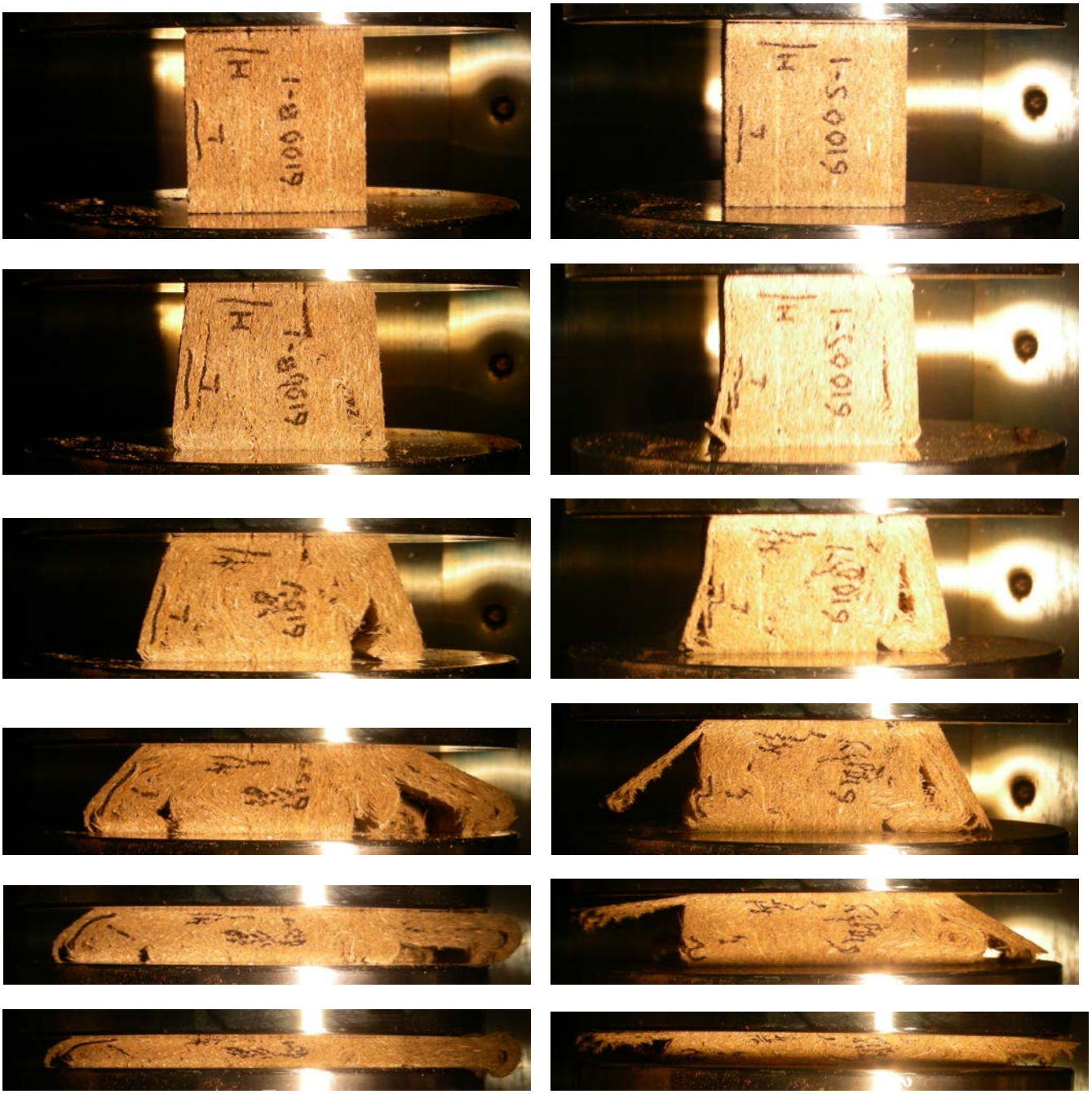

(a) Sample B1 from base of subassembly (b) Sample S1 from side of subassembly

Figure 10. Photographs of fiberboard samples during compression testing, parallel orientation

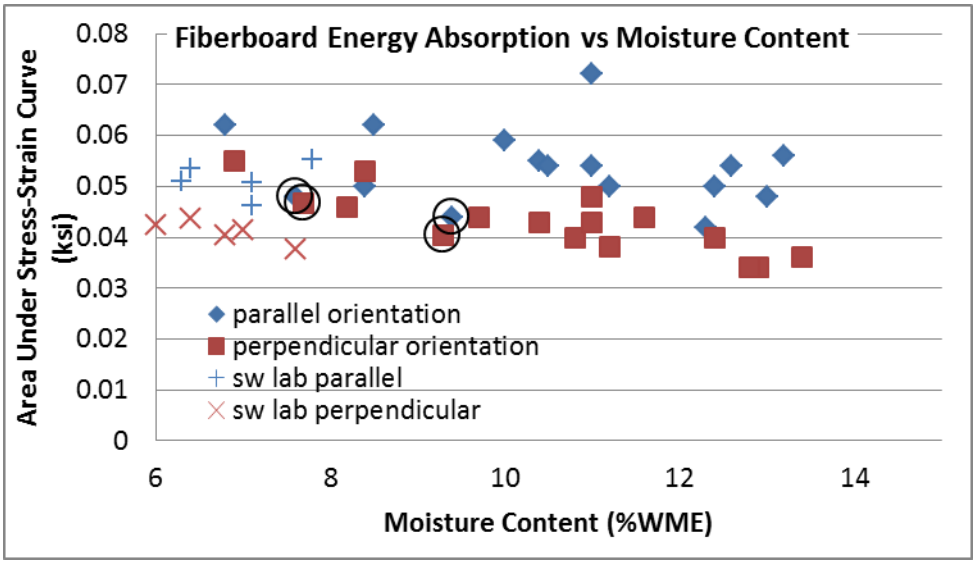

Figure 11. Fiberboard energy absorption, represented by the area under the stress-strain curve up to 40% strain, from tensile test samples from each destructively examined package (solid symbols). The results from 9975-06100 are circled. The open symbols (+, x) show baseline data from softwood fiberboard laboratory samples.

Figure 12. Jacketed lead shield.

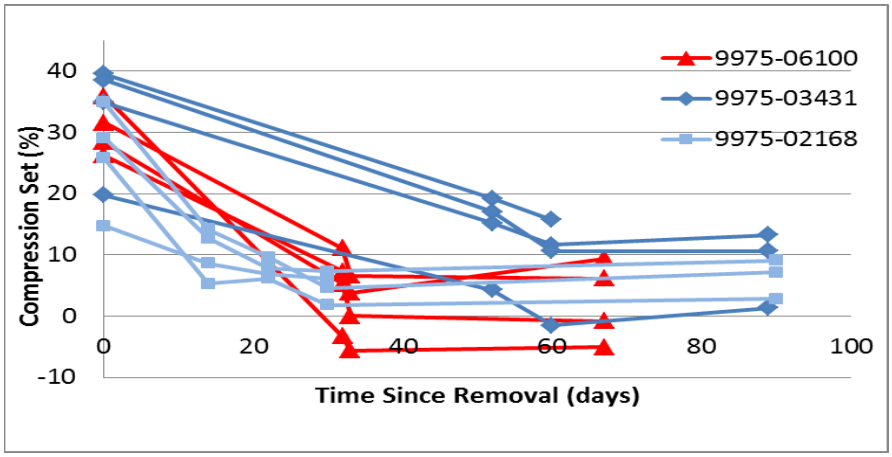

Figure 13. O-ring relaxation as indicated by change in compression set following removal during field surveillance. Results are shown for each of the 4 O-rings from 9975-06100, compared to similar data from 9975-03431 and 9975-02168.

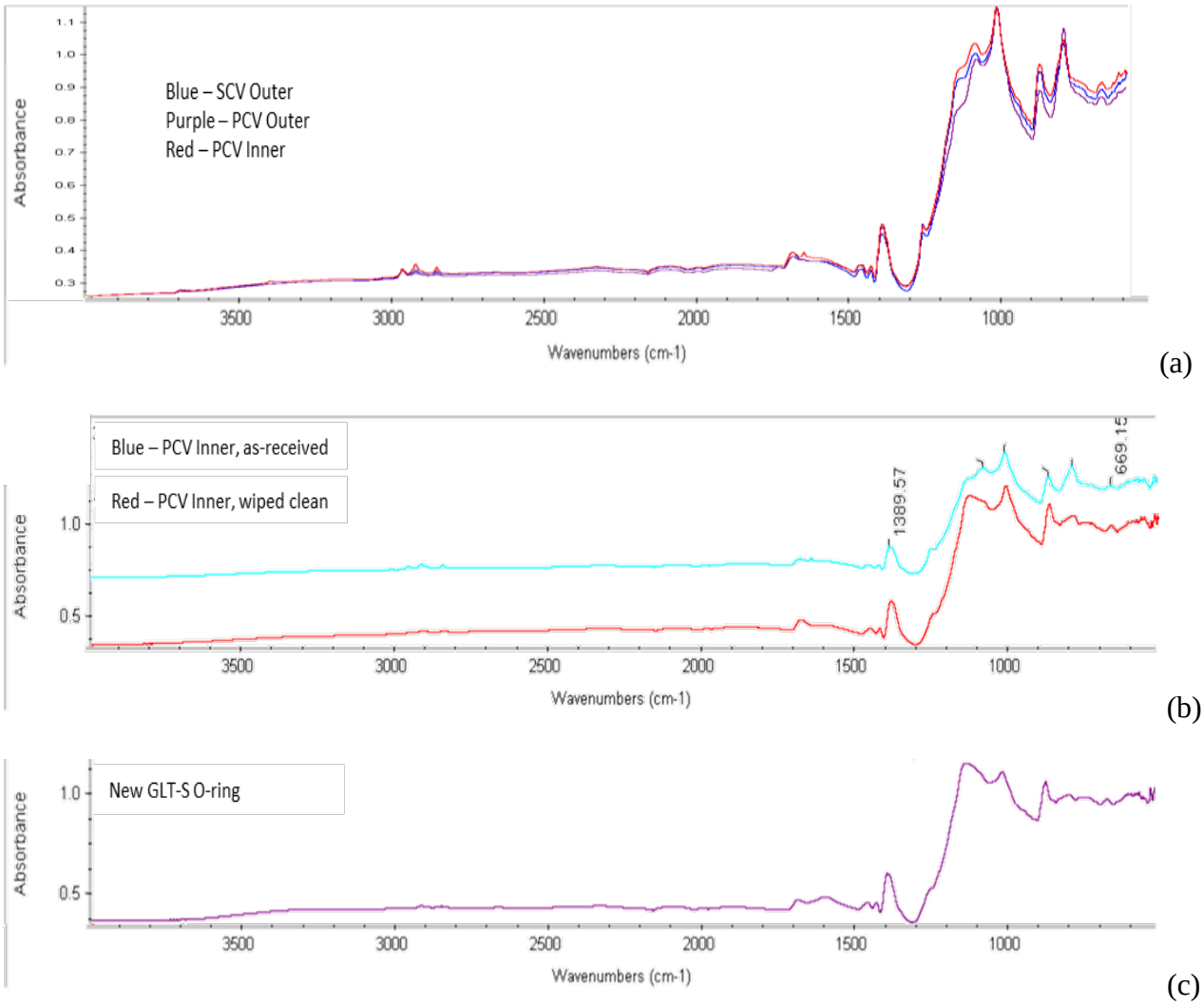

Figure 14. FT-IR spectra for the three tested Viton® GLT-S O-rings from 9975-06100, without cleaning (a). In (b), the PCV inner O-ring spectrum is repeated in the as-received condition, and compared to its spectrum after being wiped clean. A new (clean) GLT-S spectrum is shown in (c) for reference.

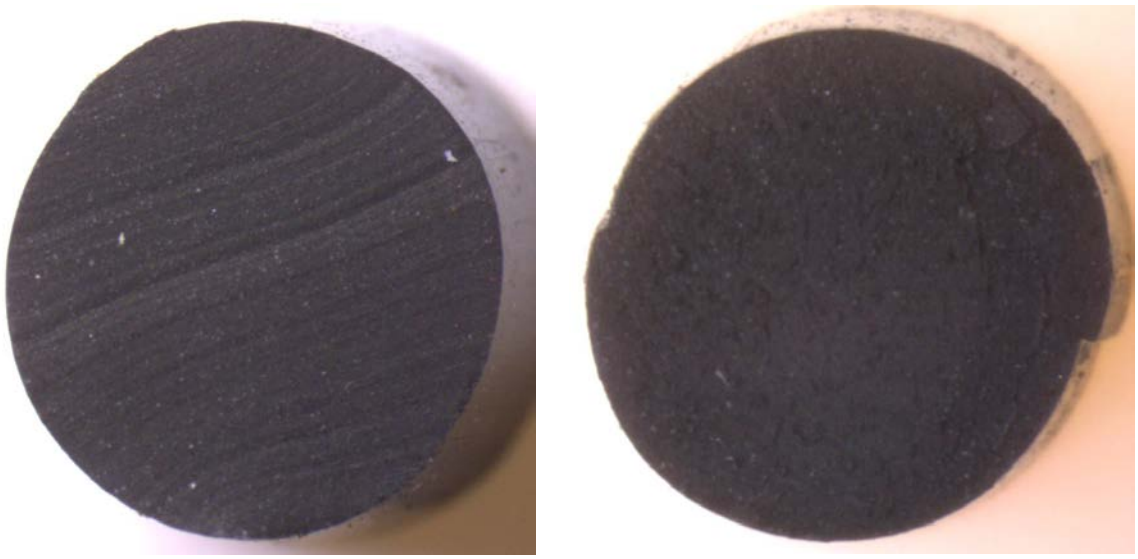

(a) (b)

Figure 15. Optical cross section of the (a) PCV outer and (b) SCV outer O-rings.

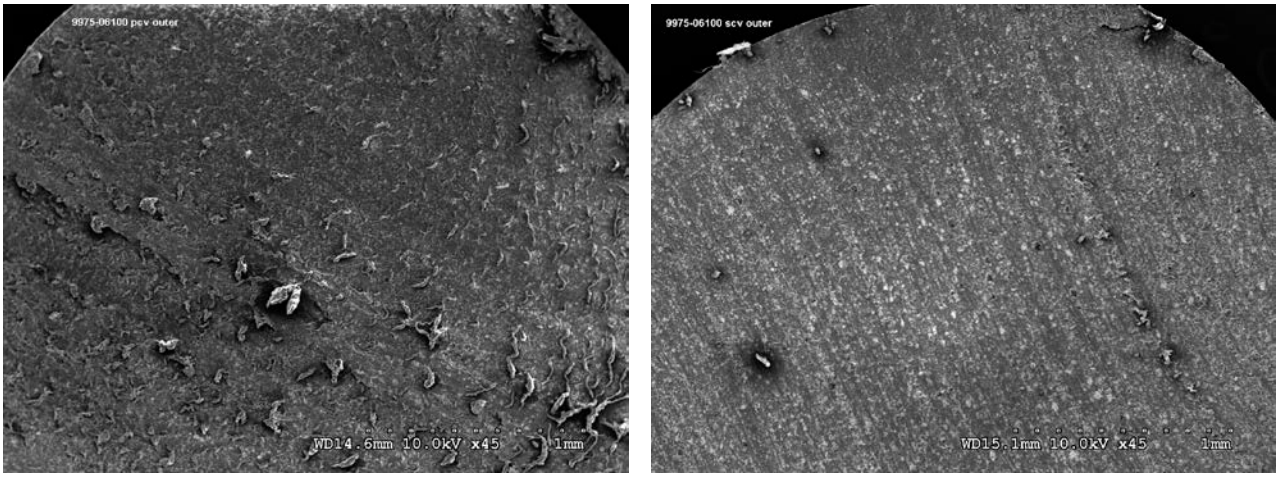

(a) (b)

Figure 16. SEM cross section of the (a) PCV outer and (b) SCV outer O-rings.

Figure 17. 9975-06100 PCV inner O-ring during tensile test, at 50% stretch.

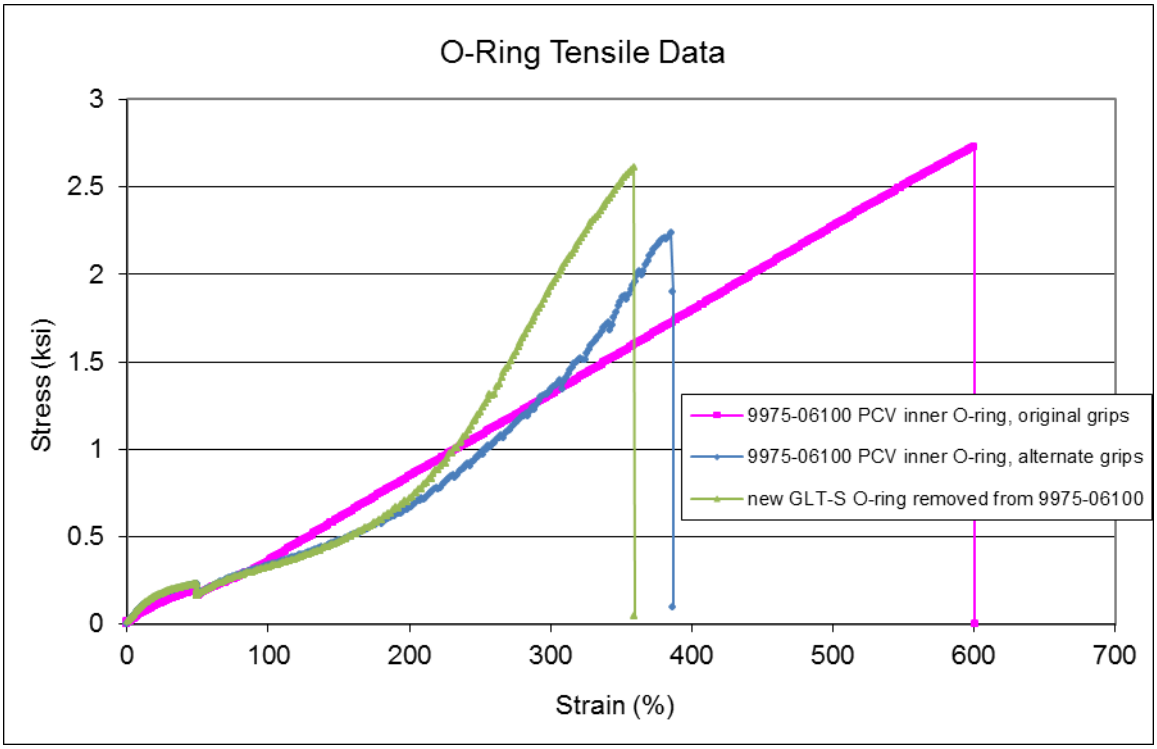

Figure 18. Tensile data for PCV inner O-ring from 9975-06100 tested with the original yarn grip configuration, with comparison curves from the same PCV inner O-ring and a new O-ring (removed from 9975-06100 PCV), both tested with a flat grip configuration.

Figure 19. Darkened surface on the interior of the SCV bottom head.

Attachment 1 9975-06100 Field Surveillance Results, with Comparison to Destructive Examination Results

Section I

Drum Exterior Examination

Item	Field Surveillance Result	Destructive Exam. Result
Drum vent plugs are specified and are in place as required	SAT	SAT
Drum surface is not dented beyond 0.25 inch	SAT	SAT
Drum Dents adjacent to the air shield are not deeper than 0.125 inch	SAT	SAT
Drum surface is free from corrosion, swelling/bulging and other physical damage	SAT	SAT

Comment – n/a

Section II

Humidity Measurements

Humidity at top of the drum	90.3 %RH	56.1 %RH

Section III

Temperature Measurements

[These data not repeated in this report.]

Section IV

Celotex® Inspection

Upper Celotex® Assembly Weight: 26.7 lb (field surv.) 12.080 kg / 26.63 lb (destructive exam)

Visual:

Item	Field Surveillance Result	Destructive Exam. Result
Inspect all exposed Celotex® surfaces for significant damage and ensure layers are well bonded	SAT	SAT
Upper Celotex® came out smoothly, without interference	SAT	SAT
All visible Celotex® surfaces are free from staining and variation in coloration	SAT	*
Celotex® is free from significant swelling (e.g. gap exists against drum), shrinkage and other significant physical damage	SAT	SAT
Lead shield is free from significant deformation and physical damage and shows no sign of flaking, blistering or spalling	SAT	SAT
Lead shield Go/No Go gauge went smoothly into the lead shield and reached all the way to the bottom of the lead shield	SAT	NA

Comments: * In destructive examination, 2 regions on the bottom of the lower fiberboard assembly with water stains. Matching stains observed on the drum bottom. The drum interior side had horizontal stains consistent with fiberboard layer contact, and vertical stains consistent with water movement. The vertical stains were not at the same circumferential positions as the fiberboard stains.

Attachment 1 9975-06100 Field Surveillance Results, with Comparison to Destructive Examination Results

Celotex® Dimensions (all results reported in inches)

Dimensions		0°	90°	180°	270°	Field Surveillance Average	Destructive Exam. Average
1	Upper Assembly OD	17.672	17.684			17.678	17.692
2	Upper Assembly lower step OD	14.682	14.722			14.702	14.732
3	Upper Assembly ID	8.512	8.508			8.510	8.532
4	Upper Assembly inside height	Not measured					5.059
5	Lower Assembly step height	Not measured					2.086
6	Lower Assembly height from lower step to top of lead shield	Not measured					NA

Dimension	Result	Criteria	Field Surveillance Result	Destructive Exam. Result
Dimension #6 average	NA	$\leq$ 4.65 "	NA	NA
Dimension #1 average – Dimension #3 average	9.168	$\geq$ 8 3/16"	SAT	SAT

Section V

O-Ring Inspection

Test	SAT/UNSAT
O-ring seal test performed on SCV	SAT
SCV O-rings were removed intact	SAT
SCV O-rings have no excess accumulation of grease	SAT
O-ring seal test performed on PCV	SAT
PCV O-rings were removed intact	SAT
PCV O-rings have no excess accumulation of grease	SAT

Comments: n/a

Attachment 1 9975-06100 Field Surveillance Results, with Comparison to Destructive Examination Results

(all dimensional results reported in inches)

Action	0°	90°	180°	270°	Time	Destructive Exam. Average Result
Loosen SCV lid					1042	NA
Outer SCV O-Ring						
Measure OD (while on plug)	6.299	6.292			1110	NA
Measure radial thickness	NM	NM	NM	NM		0.1390
Measure vertical thickness	NM					0.1369
Inner SCV O-Ring						
Measure OD (while on plug)	6.180	6.180			1110/1112	NA
Measure radial thickness	NM	NM	NM	NM		0.1364
Measure vertical thickness	NM					0.1401
Loosen PCV lid						NA
Outer PCV O-Ring						
Measure OD (while on plug)	5.249	5.248			1116/1117	NA
Measure radial thickness	NM	NM	NM	NM		0.1412
Measure vertical thickness	NM					0.1360
Inner PCV O-Ring						
Measure OD (while on plug)	5.145	5.138			1117/1119	NA
Measure radial thickness	NM	NM	NM	NM		0.1375
Measure vertical thickness	NM					0.1386

Attachment 1 9975-06100 Field Surveillance Results, with Comparison to Destructive Examination Results

SRNL Receipt Examination of O-Rings

VISUAL EXAMINATION

PCV	PCV Outer	PCV Inner
Grease present	no	no
Color (normal or explain)	Normal	Normal
Cross-sectional shape	round	round
Nicks, Scratches, Cracks	none	none
Other Damage (Note extent/size)	none	none
Picture (Note if taken)		

SCV	SCV Outer	SCV Inner
Grease (type, amount)	no	no
Color (normal or explain)	Normal	Normal
Cross-sectional shape	round	round
Nicks, Scratches, Cracks	none	none
Other Damage (Note extent/size)	none	Bubble like formation around seam
Picture (Note if taken)		

THICKNESS (all results reported in inches)

PCV	PCV Outer		PCV Inner	
	Axial	Radial	Axial	Radial
Thickness 1 (in)	0.1345	0.1395	0.1380	0.1380
Thickness 2 (in)	0.1335	0.1400	0.1395	0.1355
Thickness 3 (in)	0.1380	0.1410	0.1390	0.1350
Thickness 4 (in)	0.1380	0.1405	0.1380	0.1360
Field Surv. Average	**0.1360**	**0.1413**	**0.1386**	**0.1361**
Destructive Exam Average	**0.1360**	**0.1412**		

SCV	SCV Outer		SCV Inner	
	Axial	Radial	Axial	Radial
Thickness 1 (in)	0.1355	0.1335	0.1400	0.1323
Thickness 2 (in)	0.1350	0.1400	0.1400	0.1355
Thickness 3 (in)	0.1350	0.1375	0.1390	0.1340
Thickness 4 (in)	0.1395	0.1365	0.1405	0.1365
Field Surv. Average	**0.1363**	**0.1369**	**0.1399**	**0.1346**
Destructive Exam Average	**0.1369**	**0.1390**		

Attachment 1 9975-06100 Field Surveillance Results, with Comparison to Destructive Examination Results

SRNL Receipt Examination of O-Rings (Continued)

HARDNESS

	PCV O-Rings		SCV O-Rings	
	Outer	Inner	Outer	Inner
Hardness 1, M-Scale	85.0	83.0	83.0	82.5
Hardness 2, M-Scale	85.0	83.0	83.0	83.0
Hardness 3, M-Scale	85.0	83.0	81.5	82.5
Hardness 4, M-Scale	85.0	83.5	82.5	82.5
Hardness 5, M-Scale	85.0	83.0	83.0	83.0
Average	**85.0**	**83.1**	**82.6**	**82.7**

CONTINUATION:
NA

CC: J. S. Bellamy, 730-A
G. T. Chandler, 773-A
W. L. Daugherty, 773-A
K. A. Dunn, 773-41A
T. W. Griffin, 705-K
T. J. Grim, 105-K
E. R. Hackney, 705-K
S. J. Hensel, 705-K
D. R. Leduc, 730-A
J. W. McEvoy, 707-42B
T. E. Skidmore, 730-A
K. E. Zeigler, 773-41A
Document Control